Preprints of the 19th World Congress
The International Federation of Automatic Control
Cape Town, South Africa. August 24-29, 2014

Vision-based minimum-time planning of mobile robots with kinematic and visibility constraints

Yaozhun Huang * **Xuebo Zhang(✉)** * **Yongchun Fang** *

* *Institute of Robotics and Automatic Information System (IRAIS) and Tianjin Key Laboratory of Intelligent Robotics (tjKLIR), Nankai University, Tianjin, 300071, China. (e-mail: {zhangxb, yfang}@robot.nankai.edu.cn).*

Abstract: This paper proposes a vision-based minimum-time trajectory planning method for mobile robots, which takes into account kinematic constraints for linear/angular velocities and accelerations, as well as the visibility constraint. Different from existing methods, by means of homography-based pose estimation, the vision-based trajectory planning is formulated as a constrained optimal control problem in the scaled Euclidean space, which is solved by using the Gauss Pseudospectral Method (GPM). Specifically, the homography matrix is estimated and then decomposed to obtain the relative rotation angle and the scaled translation between the current pose and the desired one, which are expressed in the scaled Euclidean space. Then, kinematic constraints are taken into account in this space, while the visibility constraint is formulated by mapping the Euclidean homography matrix to the image space. To our best of knowledge, it is the first reported approach to solve the vision-based minimum-time trajectory planning problem for wheeled mobile robots, which can help improve the working efficiency in realistic visual servoing systems. Extensive simulation and experimental results with comparison to other related methods are presented to demonstrate the effectiveness of the proposed approach.

Keywords: Visual servoing, mobile robotics, trajectory planning

1. INTRODUCTION

Visual servoing exploits real-time image feedback to complete robot control tasks, which has been widely applied in many areas such as robot manipulators, wheeled mobile robots, unmanned aerial vehicles (UAV), see Chaumette et al. (2006); Liu et al. (2013); Guenard et al. (2008).

Sensing and actuation constraints are important when putting the visual servoing theory into practice. In particular, since a single camera has a limited field-of-view (FOV), this visibility constraint should be guaranteed to obtain available image feedback during the visual servoing process. In addition, the kinematic constraints, including the maximum linear and angular velocity of the robot, should also be taken into account in practice. These visibility and kinematic constraints, becomes even more challenging for vision-based control wheeled mobile robots (WMRs), as the complex nonholonomic constraint of WMRs makes the motion planning and controller design much more difficult, see Li et al (1993).

In order to cope with the visibility constraint, some results have been reported for visual servoing of robot manipulators by Mezouar et al (2002); Wang et al. (2012). A hybrid visual servoing (HVS) strategy is designed by Wang et al. (2012) using Lyapunov-based techniques to stabilize a robot manipulator. It should be noted that this approach achieves good performance while simultaneously satisfying practical FOV and actuation constraints.

One mainstream class of methods is to utilize a planning and control framework, for which various constraints can be taken into account in the planning stage, followed by image-based tracking control to complete visual servoing tasks such as the classical work of Mezouar et al (2002). An excellent survey of this topic can be found in Kazemi (2010) and Chesi (2009) employ convex optimization to successfully handle the visibility constraint and other geometry constraints such as work space, joint limits, occlusion, and so on. Shademan et al. (2012) and Kazemi (2012) use the methodologies from sampling-based planning to address vision-based path planning problem in the presence of robot motion and visibility constraints. The work of Kermorgant et al. (2013) uses a weighting matrix to consider the visibility and robot joint constraints. Yet, these methods usually regard the robot end-effector as a freely moving point in its allowable workspace, which dose not take into account the nonlohonomic constraint for wheeled mobile robots. In addition, these approaches generally focus on the path planning level, and optimal trajectory planning which should also consider the kine-

⋆ This work is supported in part by National Natural Science Foundation of China under Grant 61203333, in part by Specialized Research Fund for the Doctoral Program of Higher Education of China under Grant 20120031120040, in part by Tianjin Natural Science Foundation under Grant 13JCQNJC03200.

matic constraints such as maximum velocities, needs to be further studied.

Restricting the topic to visual servoing of mobile robots, the control problem becomes more challenging due to the well-known nonholonomic constraints. Zhang et al. (2011) propose a motion estimation method which only requires a small number of features to alleviate the FOV problem, while Fang et al. (2012) utilize active pan-tilt camera to keep features visible during the servoing process. Bhattacharya et al (2007) propose an optimal path planning approach which successfully yields the shortest path length under the visibility constraint, and López-Nicolás et al (2009) further propose a novel visual control approach using feedback of homography elements. The work of Salaris et al. (2010) presents an advanced optimal planning method which successfully consider both Horizontal-FOV(H-FOV) and Vertical-FOV(V-FOV) constraints. Note that these methodologies are important in practice and can yield the shortest-length path, the research on minimum-time planning of wheeled mobile robots under FOV and kinematic constraints are still open.

To increase the servoing efficiency, this paper makes an attempt to give a solution to the vision-based minimum-time trajectory planning problem, in the presence of limited field-of-view (FOV) and kinematic constraints for maximum linear/angular velocities and accelerations. In particular, a mobile robotic system with a fixed onboard camera is considered, with a previously captured desired image representing the target pose of the mobile robot. During the planning process, the homography matrix between the current image and the desired one is estimated and then decomposed to obtain a relative orientation and a scaled translation. Subsequently, we successfully formulate minimum-time trajectory planning problem into a constrained optimal control problem in the scaled Euclidean space. In this formulation, FOV and kinematic constraints can be taken into account by using the relationship between the homography matrix and the relative pose to obtain the mapping between the scaled Euclidean space and the image space. Afterwards, Gauss pseudospectral method(GPM) is adopted to numerically solve this optimal control problem, since GPM has a fast convergence rates than other pseudospectral methods. Extensive simulation and experimental results in comparison with shortest-path planning (SPP) are presented to demonstrate superior performance of the proposed approach.

2. PROBLEM STATEMENT

Consider a mobile robot with a fixed onboard camera, let $\mathcal{F}_c$ denote a right-hand camera frame, with its X_c axis being the optical axis pointing to the front of the mobile robot. The Z_c axis is perpendicular to the motion plane of the mobile robot and passes through the midpoint of the wheels axis. The camera frame at the desired pose is defined as the desired camera frame $\mathcal{F}_c^*$ which is regarded as the world reference frame in this paper.

2.1 Homography-based pose estimation

For a planar reference object, the relationship between the current image and the desired one is described by a projective homography matrix $\boldsymbol{G} \in \mathbb{R}^{3\times3}$:

$$\boldsymbol{p}_i = \lambda_i \boldsymbol{G} \boldsymbol{p}_i{}^* \tag{1}$$

where $\boldsymbol{p}_i = [1 \quad u_i \quad v_i]^{\mathrm{T}}$, $\boldsymbol{p}_i^* = [1 \quad u_i^* \quad v_i^*]^{\mathrm{T}} \in \mathbb{R}^3$ represent image pixel coordinates of feature points $\mathcal{P}_i$ $(i = 1, 2 \dots N)$, in the current image I and the desired image I^*, respectively. $\lambda_i \in \mathbb{R}$ is a scale factor. Note that $\boldsymbol{G}$ encodes the information for both camera internal and external parameters. To obtain the relative pose between $\mathcal{F}_c$ and $\mathcal{F}_c^*$, a Euclidean homography matrix $\boldsymbol{H}$ is obtained as follows:

$$\boldsymbol{H} = \boldsymbol{A}^{-1} \boldsymbol{G} \boldsymbol{A} \tag{2}$$

where $A \in \mathbb{R}^{3\times3}$ is the camera intrinsic matrix. The matrix $\boldsymbol{H}$ is further decomposed as

$$\boldsymbol{H} = \boldsymbol{R} + \frac{\boldsymbol{T}}{d^*} \boldsymbol{n}^{*T} \tag{3}$$

where $\boldsymbol{R} \in \mathbb{R}^{3\times3}$ and $\boldsymbol{T} \in \mathbb{R}^3$ denote the rotation matrix and translation vector between $\mathcal{F}_c$ and $\mathcal{F}_c^*$. $\boldsymbol{n}^* = [n_x{}^*, n_y{}^*, n_z{}^*]^T \in \mathbb{R}^3$ is the normal vector of the reference plane expressed in $\mathcal{F}_c^*$, and $d^* \in \mathbb{R}$ is the distance between origin of $\mathcal{F}_c^*$ and the reference plane. To facilitate the subsequent analysis, a scaled translation vector $\boldsymbol{t} = [t_x \quad t_y \quad 0]^{\mathrm{T}} \in \mathbb{R}^3$ is introduced as follows:

$$\boldsymbol{t} = \frac{\boldsymbol{T}}{d^*} \tag{4}$$

By using feature point matching between the current image and the desired one, the matrix $\boldsymbol{G}$ can be computed. Afterwards, the homography matrix $\boldsymbol{H}$ is obtained using the calibrated camera intrinsic matrix $\boldsymbol{A}$ and (2). Then, $\boldsymbol{R}$, $\boldsymbol{t}, \boldsymbol{n}^*$ of the robot can be obtained by decomposition of the homography, see Chen et al (2006). Using the rotation matrix $\boldsymbol{R}$, it is easy to obtain the rotational angle $\theta \in (-\pi, \ \pi]$ as

$$\theta_d = \operatorname{atan2}(r_{21}, \ r_{11}) \tag{5}$$

with $r_{ij} \in \mathbb{R}$ being the i^{th}-row, j^{th}-column entry of $\boldsymbol{R}$. In the following, we aims to plan a trajectory for the measurable signals θ and $\boldsymbol{t} = [t_x \quad t_y \quad 0]^{\mathrm{T}}$ in the scaled Euclidean space.

2.2 System model development

In terms of the scaled translation $\boldsymbol{t} = [t_x \quad t_y \quad 0]^{\mathrm{T}}$ and the rotation angle θ, the kinematics model of a unicycle mobile robot is described as

$$\begin{cases} \dot{t}_x = \dfrac{\upsilon}{d^*} \cos(\theta) \\ \dot{t}_y = \dfrac{\upsilon}{d^*} \sin(\theta) \\ \dot{\theta} = \omega \end{cases} \tag{6}$$

where $\upsilon \in \mathbb{R}$ and $\omega \in \mathbb{R}$ denote the linear velocity and the angular velocity, respectively. Note that $d^* \in \mathbb{R}$ is an unknown constant denoting the distance between origin of $\mathcal{F}_c^*$ and the reference plane.

The objective of the paper is to first plan a minimum-time trajectory θ_d and $\boldsymbol{t}_d = [t_{xd} \quad t_{yd} \quad 0]^{\mathrm{T}}$ for measurable signals θ and $\boldsymbol{t} = [t_x \quad t_y \quad 0]^{\mathrm{T}}$, and then we will use the kinematic model (11) to make the robot track the planned reference trajectory such that

$$\lim_{t\to\infty} (\boldsymbol{t} - \boldsymbol{t}_d) = 0, \ \lim_{t\to\infty} (\theta - \theta_d) = 0. \tag{7}$$

To discriminate notation for planned trajectories and the current system state, we use the subscript $(\cdot)_d$ in the rest of the paper to denote the variables relating to planned trajectories.

3. GPM-BASED MINIMUM-TIME TRAJECTORY PLANNING

To satisfy the velocity and acceleration constraints, we propose an augmented system model, based on which the kinematic and visibility constraints are expressed as functions of system state or control varaibles. Subsequently, the minimum-time trajectory planning problem is converted into a constrained time-optimal control problem, which is further solved by using GPM.

3.1 Augmented System Model

Since the constant distance d^* is unknown, we introduce a scaled linear velocity $v^* \in \mathbb{R}$ as follows:

$$v^* = \frac{v}{d^*}. \tag{8}$$

By using the subscript $(\cdot)_d$ for planned trajectories, the kinematic model becomes

$$\begin{cases} \dot{t}_{xd} &= v_d^* \cos(\theta_d) \\ \dot{t}_{yd} &= v_d^* \sin(\theta_d) \\ \dot{\theta}_d &= \omega_d \end{cases} \tag{9}$$

To satisfy the acceleration constraints and simultaneously ensure high-order smoothness of planned trajectories for $t_{xd}(t),\ t_{yd}(t),\ \theta_d(t)$, the system state is augmented by using the derivative of scaled linear acceleration and angular acceleration, i.e. scaled linear jerk and angular jerk, as the new control input vector.

Let a_{vd}^* and j_{vd}^* being the scaled linear acceleration and scaled linear jerk, with $a_{\omega d}$ and $j_{\omega d} \in \mathbb{R}$ being the angular acceleration and angular jerk, respectively. Then we have

$$a_{vd}^* = \dot{v}_d^*, \quad j_{vd} = \dot{a}_{vd}^*, \quad a_{\omega d} = \dot{\omega}_d, \quad j_{\omega d} = \dot{a}_{\omega d}. \tag{10}$$

Therefore, the augmented system model is obtained:

$$\begin{cases} \dot{t}_{xd} &= v_d^* \cos(\theta_d) \\ \dot{t}_{yd} &= v_d^* \sin(\theta_d) \\ \dot{\theta}_d &= \omega_d \\ \dot{v}_d^* &= a_{vd}^* \\ \dot{\omega}_d &= a_{\omega d} \\ \dot{a}_{vd}^* &= j_{vd}^* \\ \dot{a}_{\omega d} &= j_{\omega d} \end{cases} \tag{11}$$

which can be rewritten as the following form

$$\dot{\boldsymbol{\xi}}(t) = f(\boldsymbol{\xi}(t), \boldsymbol{u}(t), t), \quad t \in [t_0, t_f], \tag{12}$$

with the system state $\boldsymbol{\xi}(t) \in \mathbb{R}^7$ and control input vector $\boldsymbol{u}(t) \in \mathbb{R}^2$ being $\boldsymbol{\xi} = [t_{xd} \ \ t_{yd} \ \ \theta_d \ \ v_d^* \ \ \omega_d \ \ a_{vd}^* \ \ a_{\omega d}]^T$, $\boldsymbol{u}(t) = [j_{vd}^* \ \ j_{\omega d}]^T$. In the following, the problem is converted to find the optimal control input $\boldsymbol{u}(t)$ to drive the mobile robot from the initial position to the origin while satisfying state and control constraints, path constraints as well as the boundary conditions. When the control input trajectory $\boldsymbol{u}(t)$ is determined, the trajectories for $t_{xd}(t),\ t_{yd}(t),\ \theta_d(t),\ \dot{t}_{xd}(t),\ \dot{t}_{yd}(t),\ \dot{\theta}_d(t)$ can be computed simultaneously using the GPM in section 3.4.

3.2 Constraints

Boundary Constraints For the vision-based trajectory planning task, boundary conditions should be satisfied for the initial configuration $\xi(t_0)$ and the desired one $\xi(t_f)$:

$$\boldsymbol{\xi}(t_0) = [t_{xd0}, t_{yd0}, \theta_{d0}, 0, 0, 0, 0]^T \tag{13}$$

$$\boldsymbol{\xi}(t_f) = [0, 0, 0, 0, 0, 0, 0]^T \tag{14}$$

where $t_{xd0},\ t_{yd0} \in \mathbb{R}$ represent the initial position, with $\theta_{d0} \in (-\pi,\ \pi]$ being the initial orientation. $t_0,\ t_f \in \mathbb{R}$ denote the starting time and the arrival time, respectively. Since the desired pose is set as the reference frame, the desired configuration should be at the origin.

Statement and Control Constraints In practice, the visual servoing task, as well as the motor physical limits, enforces several kinematic constraints such as the maximum linear/angular velocity and the maximum linear/angular acceleration. These practical motion constraints are expressed as follows:

$$-\frac{v_{max}}{\bar{d}^*} \le v_d^*(t) \le \frac{v_{max}}{\bar{d}^*} \tag{15}$$

$$-\frac{a_{vmax}}{\bar{d}^*} \le a_{vd}^*(t) \le \frac{a_{vmax}}{\bar{d}^*} \tag{16}$$

$$-\omega_{max} \le \omega_d(t) \le \omega_{max} \tag{17}$$

$$-a_{\omega max} \le a_{\omega d}(t) \le a_{\omega max} \tag{18}$$

where $v_{max}, \omega_{max} \in \mathbb{R}^+$ are defined as the maximum linear velocity and maximum angular velocity of the mobile robot system, respectively; $a_{vmax}, a_{\omega max} \in \mathbb{R}^+$ are the maximum linear acceleration and maximum angular acceleration of the system. $\bar{d}^* \in \mathbb{R}$ is a known upper bound of the unknown distance d^*. Note that state constraints for $v_d^*(t)$ and $a_{vd}^*(t)$ are given in a robust manner, by using the upper bound to ensure the planned trajectory can be implemented in practice.

In addition, to ensure that the accelerations do not change too fast, the magnitude of the jerk control input is constrained in an appropriate range as

$$-\boldsymbol{u}_{max} \le \boldsymbol{u}(t) \le \boldsymbol{u}_{max} \tag{19}$$

with $\boldsymbol{u}_{max} = [j_{vmax}^* \ \ j_{\omega max}]^{\mathrm{T}}$.

Path Constraints During the visual servoing process, visibility constraints, which mean that features should always lie in the camera field of view, needs to be guaranteed to obtain effective visual feedback. By means of the relationship (3) between the homography matrix $\boldsymbol{H}$ and the planned orientation θ_d and scaled translation $t_{xd},\ t_{yd}$, the visibility constraint is can be formulated using the system state.

It follows from (2) that

$$\boldsymbol{G} = \boldsymbol{A}\boldsymbol{H}\boldsymbol{A}^{-1}. \tag{20}$$

Substituting (3) and (4) into (20) yields

$$\boldsymbol{G} = \boldsymbol{A}(\boldsymbol{R}_d + \boldsymbol{t}_d \boldsymbol{n}^{*T})\boldsymbol{A}^{-1}. \tag{21}$$

where $\boldsymbol{R}_d$ is the rotation matrix recovered from the rotation angle θ_d, with $\boldsymbol{t}_d = [t_{xd} \ \ t_{yd}]^{\mathrm{T}}$. Since feature pixel coordinates $\boldsymbol{p}_i^* = [1 \ \ u_i^* \ \ v_i^*]^{\mathrm{T}}$ at the desired pose is known, the corresponding feature pixel coordinates at the current pose can be acquired using (1) as

$$\boldsymbol{p}_i = \lambda_i \boldsymbol{A}(\boldsymbol{R}_d + \boldsymbol{t}_d \boldsymbol{n}^{*T})\boldsymbol{A}^{-1}\boldsymbol{p}_i^*. \tag{22}$$

Therefore, by introducing unit vectors $\boldsymbol{j}_1 = [1 \ \ 0 \ \ 0]^{\mathrm{T}}$, $\boldsymbol{j}_2 = [0 \ \ 1 \ \ 0]^{\mathrm{T}}$ and $\boldsymbol{j}_3 = [0 \ \ 0 \ \ 1]^{\mathrm{T}}$, λ_i is calculated as:

$$\lambda_i = \boldsymbol{j}_1^{\mathrm{T}} \boldsymbol{A}(\boldsymbol{R}_d + \boldsymbol{t}_d \boldsymbol{n}^{*T})\boldsymbol{A}^{-1}\boldsymbol{p}_i^* \tag{23}$$

λ_i is a scale factor to normalize the first element of $\boldsymbol{p}_i$ to be 1. Based on (22) and (23), the visibility constraints are expressed with a form of path constraints as follows:

$$\begin{cases} 0 \leq \dfrac{\boldsymbol{j}_2^{\mathrm{T}} \boldsymbol{A}(\boldsymbol{R}_d + \boldsymbol{t}_d \boldsymbol{n}^{*T}) \boldsymbol{A}^{-1} \boldsymbol{p}_i^*}{\boldsymbol{j}_1^{\mathrm{T}} \boldsymbol{A}(\boldsymbol{R}_d + \boldsymbol{t}_d \boldsymbol{n}^{*T}) \boldsymbol{A}^{-1} \boldsymbol{p}_i^*} \leq w \\ 0 \leq \dfrac{\boldsymbol{j}_3^{\mathrm{T}} \boldsymbol{A}(\boldsymbol{R}_d + \boldsymbol{t}_d \boldsymbol{n}^{*T}) \boldsymbol{A}^{-1} \boldsymbol{p}_i^*}{\boldsymbol{j}_1^{\mathrm{T}} \boldsymbol{A}(\boldsymbol{R}_d + \boldsymbol{t}_d \boldsymbol{n}^{*T}) \boldsymbol{A}^{-1} \boldsymbol{p}_i^*} \leq h \end{cases} \tag{24}$$

where $w,\ h \in \mathbb{R}$ denote the width and height of the image in pixels, respectively. So far, we have successfully transcribe the visibility constraints to path constraints on the system state $\theta_d,\ t_{xd},\ t_{yd}$, which is subsequently taken into account in the constrained optimal control framework.

3.3 Formulation of the minimum-time trajectory planning problem

With the previous developed system model and constraints, the minimum-time trajectory planning problem can be formulated as a constrained time-optimal control problem. The mathematical formulation is given as:

$$\min_{\boldsymbol{u}(t) \in \boldsymbol{U}} \quad J = t_f - t_0, \tag{25}$$

subject to (12), (13),(14),(15), (16), (17), (18), (19) and (24). where $J \in \mathbb{R}$ represent the total planning time. By solving this constrained time optimal control problem, the optimal trajectories for both the control input $\boldsymbol{u}(t)$ and the system state $\boldsymbol{\xi}(t)$ are computed.

3.4 GPM-based minimum-time trajectory planning

The vision-based trajectory planning has been formulated as a constrained optimal control problem. In this section, Gauss Pseudospectral Method(GPM) is directly adopted to give an effective solution. For more details, please refer to Rao et al. (2010).

The main idea of GPM is described as follows. The Legendre-Guass (LG) points are used to discretize the state and control trajectories, which are then approximated by Lagrange interpolating polynomials using the value of the state and control variables at these specific LG points. Hence, the derivative of the state trajectory can be approximated by directly differentiating the Lagrange polynomials, thus the system dynamics equations are converted to algebraic equations. In addition, the terminal state can be approximated by using Guass quadrature. *As a consequence, the time optimal control becomes a parametric nonlinear programming problem (NLP) subject to a series of algebraic constraints.* By further solving this NLP using sequence quadratic programming (SQP), trajectories for the control input $\boldsymbol{u}(t)$ and the system state $\boldsymbol{\xi}(t)$ can be computed. The resulting trajectories for $t_{xd}(t),\ t_{yd}(t),\ \theta_d(t),\ \dot{t}_{xd}(t),\ \dot{t}_{yd}(t),\ \dot{\theta}_d(t)$ are then utilized as reference trajectories for the subsequent visual servo tracking controller.

4. SIMULATION RESULTS

To demonstrate the effectiveness of the proposed vision-based minimum-time trajectory planning method, simulation results are provided. The GPOPS software package and the SNOPT tool for SQP are utilized to implement the GPM algorithm. In the simulation, the kinematic constraints and $\bar{d}^*$ are set as follows:

$$v_{max} = 0.5 \text{ m/s}, \quad \omega_{max} = 0.5 \text{ rad/s}, \quad \bar{d}^* = 1.5\text{m} \tag{26}$$

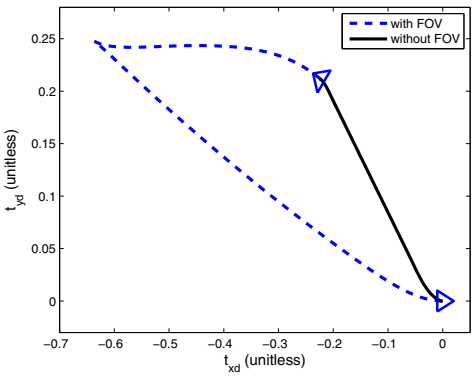

Fig. 1. Trajectories with/without the FOV constraint

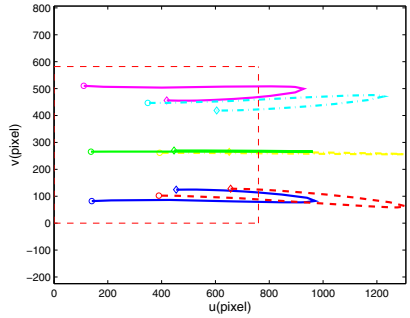

(a)

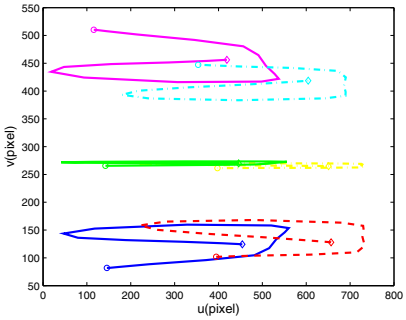

(b)

Fig. 2. (a) Pixel trajectories without the FOV constraint, where the dashed rectangle (red) denotes the camera FOV. (b) Pixel trajectories with the FOV constraint

$$a_{vmax} = 0.3 \text{ m/s}^2, \quad a_{\omega max} = 1.0 \text{ rad/s}^2 \tag{27}$$

$$j^*_{vmax} = 100\text{m/s}^3, \quad j_{\omega max} = 100 \text{ rad/s}^3 \tag{28}$$

For the camera with a limited FOV, the internal parameters are set as $u_0 = 376.9,\ v_0 = 285.3,\ f_x = 1003.7,\ f_y = 1006.3$, with its resolution being $w = 760$ pixels and $h = 582$ pixels. Six reference points are chosen as the features to increase the accuracy for the homography estimation. In all these simulation results, the origin $[t_{xd}\ \ t_{yd}\ \ \theta_d]^{\mathrm{T}} = [0\ \ 0\ \ 0]^{\mathrm{T}}$ is the desired configuration.

4.1 Results with and without visibility constraints

One main factor that affects the planning result is the visibility constraint. Hence, it is interesting to investigate the behavior of planning results using a limited FOV camera compared with those not considering visibility constraints.

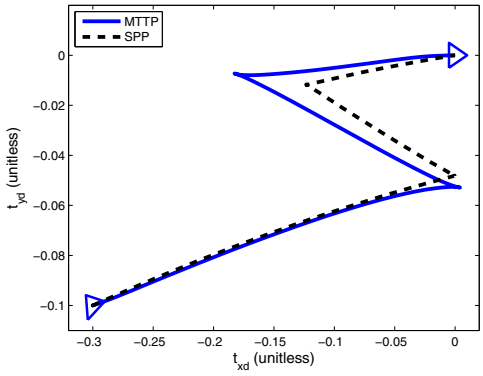

Fig. 3. The solid line (blue) denotes the trajectory by MTTP, the dashed line (black) is the trajectory by SPP.

Table 1. comparison of path length and time between two methods

	Path Length(unitless)	Time(s)
MTTP	0.683	5.277
SPP	0.559	11.927

When visibility constraints are not considered, the mobile robot can move more freely, and resulting paths are short. To ensure visibility constraints, the minimum-time trajectories may become longer when lateral error is larger. One comparative example is shown in Figure 1. The solid line (black) denotes the motion trajectory without considering FOV, while the dashed line (blue) represents the trajectory considering the FOV constraint. Figure 2 shows the corresponding pixel trajectories result without and with the visibility constraint. It is shown that, though the result without visibility constraints presents more efficient trajectories, the feature points may escape outside the camera field of view.

4.2 Comparison with shortest-path planning

In order to further illustrate the performance of the proposed minimum-time trajectory planning method (MTTP), we conduct comparative simulation with respect to the shoretest-path planning (SSP) considering visibility constraints [1] . It is found that these two types of trajectories are not always closed to each other, and in some cases, they are obviously different. Hence, it is necessary to study the MTTP to improve the visual servo efficiency.

One example is given in Figure 3, wherein the solid line denotes results for MTTP and the dashed line represent the one for SSP. It is seen that though the resultant path for MTTP is longer than the one for SSP, MTTP is much more efficient as shown in Table 1.

5. EXPERIMENTAL RESULTS

In the experiments, we use the proposed MTTP to plan the minimum-time trajectories for $t_{xd}(t)$, $t_{yd}(t)$, $\theta_d(t)$, $\dot{t}_{xd}(t)$, $\dot{t}_{yd}(t)$, $\dot{\theta}_d(t)$, while these trajectories are tracked by directly employing the visual servo tracking approach in the work of Chen et al (2006).

[1] The SSP is implemented by setting the objective function of the proposed approach as $\int_0^{t_f} |v_d^*(t)|$.

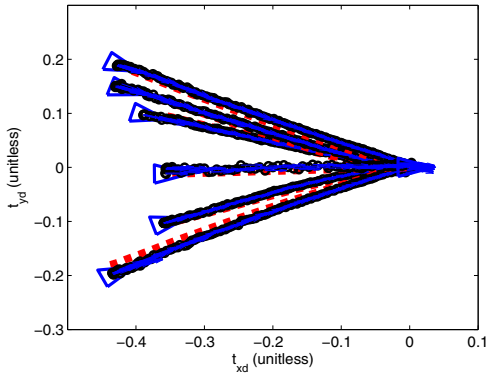

Fig. 4. Planned trajectories (red dashed lines) and actual trajectories (blue solid lines) with small lateral errors.

A PD-3X mobile robot is utilized in the experiment, with kinematic constraints, $\bar{d}^*$ and camera parameters being set as same as those in the simulation.

Figure 4 shows several resulting trajectories from different initial poses, wherein dashed trajectories (red) are planned by MTTP, and the solid trajectories (blue) are real trajectories using visual feedback. It is seen that the tracking controller works well with small tracking errors. From Figure 4, it is also shown that with small lateral translation between the initial pose and the desired one, the length of minimum-time trajectories are also short.

However, when the lateral translation along Y_c axis increases, the trajectories become much more complicated since it is hard to keep the features in FOV if the robot moves along a short path. One of the experimental results is shown in Figure 5 (a). During the tracking process, the arrows may not be precisely along the forward directions of the mobile robot, because the arrows are calculated by homography-based pose estimation where some small errors are unavoidable due to image noises. Though some arrows are slightly inconsistent with the moving directions at some locations, it is generally right in most cases.

5.1 Experimental Comparison with SSP

Comparative experimental results between MTTP and SPP are also presented to illustrate the difference of these two type of methods. By using the same initial configurations of the proposed MTTP as shown in Figure 5 (a), we present comparative results of SPP in Figure 5 (b). The time performance are shown in Tab. 2. These results reveal again that the results by MTTP have large difference from the SSP, and it should be paid attention to improve the efficiency of practical visual servoing systems, even at the price of longer motion paths.

6. CONCLUSION

This paper presents a vision-based minimum-time trajectory planning approach for wheeled mobile robots in presence of visibility and kinematic contraints. Different from existing methods, the vision-based minimum-time trajectory planning problem is formulated as a constrained time-optimal control problem in the scaled Euclidean space, wherein the visibility constraints is established by

Table 2. comparison of path length and time between two methods

	Planned Path Length (unitless)	Actual Path Length (unitless)	Planned Time (s)	Actual Time (s)
MTTP	1.597	1.351(1.752(unit:m))	9.299	10.494
SPP	1.167	1.1632(1.495(unit:m))	14.158	15.053

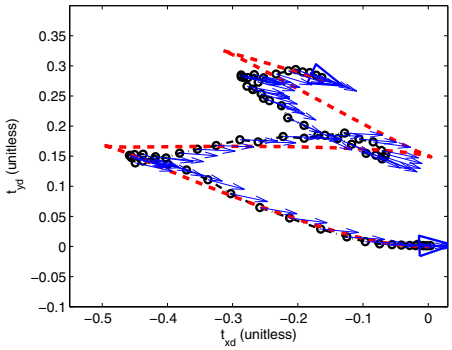

(a) MTTP

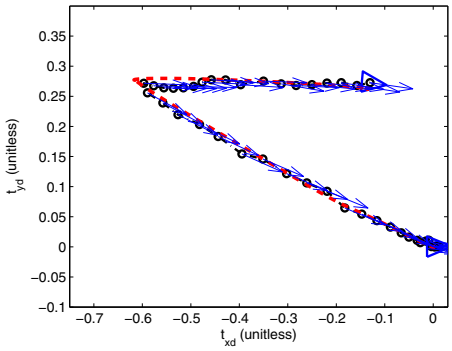

(b) SPP

Fig. 5. Planned trajectory (red dashed line) and actual trajectory (blue solid line) with larger lateral errors.

using the homography matrix to map the scaled pose information to the image space. Afterwards, GPM is utilized to successfully give an effective solution. To our best of knowledge, it is the first approach to solve the vision-based minimum-time trajectory planning problem for mobile robots, which can help improve the working efficiency in realistic visual servoing systems. Simulation and experimental results are provided, which illustrate the effectiveness of the proposed method. Future work will focus on extending the proposed method to deal with other practical constraints, such as the obstacle avoidance, occlusion, and so on.

REFERENCES

Y. Liu, H. Wang, W. Chen, D. Zhou. Adaptive visual servoing using common image features with unknown geometric parameters. *Automatica*, 2013, 49(8):2453–2460.

F. Chaumette, S. Hutchinson. Visual servo control. I. Basic approaches. *IEEE Robotics & Automation Magazine*, 2006, 13(4):82–90.

N. Guenard, T. Hamel, R. Mahony. A practical visual servo control for an unmanned aerial vehicle. *IEEE Trans. on Robotics*, 2008, 24(2):331–340.

Y. Fang, X. Liu, X. Zhang. Adaptive active visual servoing of nonholonomic mobile robots. *IEEE Trans. on Industrial Electronics*, 2012, 59(1):486–497.

X. Zhang, Y. Fang, X. Liu. Motion-estimation-based visual servoing of nonholonomic mobile robots. *IEEE Trans. on Robotics*, 2011, 27(6):1167–1175.

X. Zhang, Y. Fang, N. Sun. Visual servoing of mobile robots for posture stabilization: from theory to experiments. *International Journal of Robust and Nonlinear Control*, 2013, online published, DOI: 10.1002/rnc.3067.

J. Chen, W. Dixon, D. Dawson, and M. McIntyre. Homography-based visual servo tracking control of a wheeled mobile robot. *IEEE Trans. on Robotics*, 2006, 22(2):407–416.

Z. Wang, D. J. Kim, and A. Behal. Design of stable visual servoing under sensor and actuator constraints via a Lyapunov-based approch. *IEEE Trans. on Control Systems Technology*, 2012, 20(6):1575–1582.

Y. Mezouar, F. Chaumette. Path planning for robust image-based control. *IEEE Trans. on Robotics and Automation*, 2002, 18(4):534–549.

G. Chesi. Visual servoing path planning via homogeneous forms and LMI optimizations. *IEEE Trans. on Robotics*, 2009, 25(2):281–291.

G. López-Nicolás, N. Gans, S. Bhattacharya, C. Sagüés, J.J. Guerrero, S. Hutchinson. Homography-based control scheme for mobile robots with nonholonomic and field-of-view constraints. *IEEE Trans. on Systems, Man, and Cybernetics, Part B: Cybernetics*, 2009, 39(6):1–13.

S. Bhattacharya, R. Murrieta-Cid, S. Hutchinson. Optimal paths for landmark-based navigation by differential-drive vehicles with field-of-view constraints. *IEEE Trans. on Robotics*, 2007, 23(1):47–59.

M. Kazemi, K. Gupta, M. Mehrandezh. Visual servoing via advanced numerical methods, ser. *Lecture Notes in Control and Information Sciences (LNCIS 401)*. Springer, 2010:189–207.

M. Kazemi, K.K. Gupta, M. Mehrandezh. Randomized kinodynamic planning for robust visual servoing. *IEEE Trans. on Robotics*, 2013, 29(5):1197–1211.

A. Shademan, M. Jagersand. Robust sampling-based planning for uncalibrated visual servoing. *Int. Conf. on Intelligent Robots and Systems*, 2012:2663–2669.

O. Kermorgant, F. Chaumette. Dealing With Constraints in Sensor-Based Robot Control. *IEEE Trans. on Robotics*, 2013, online.

Z. Li, J. Canny, eds. Nonholonomic motion planning. vol. 192, Springer, 1993.

A. Burlacu, C. Lazar. Reference trajectory based visual predictive control. *Advanced Robotics*, 2012, 26(8-9): 1035–1054.

P. Salaris, A. Cristofaro, L. Pallottino, A. Bicchi. Hortest paths for wheeled robots with limited Field-Of-View:introducing the vertical constraint. *IEEE Trans. on Robotics*, 2010, 26(2):269–281.

A. V. Rao, D. A. Benson, C. L. Darby, M. A. Patterson, C. Francolin, I. Sanders, G. T. Huntington. Algorithm 902: GPOPS, a MATLAB software for solving multiple-phase optimal control problems using the gauss pseudospectral method. *ACM Transactions on Mathematical Software* 37(2):article 22, 39 pages, 2010.